Acoustic Structure Inverse Design and Optimization Using Deep Learning

Xuecong Sun
Key Laboratory of Noise and Vibration Research, Institute of Acoustics, Chinese Academy of Sciences
Han Jia (hjia@mail.ioa.ac.cn)
Institute of Acoustics, Chinese Academy of Sciences, 21 Beisihuanxilu Road
Yuzhen Yang
Institute of Acoustics
Han Zhao
Key Laboratory of Noise and Vibration Research, Institute of Acoustics, Chinese Academy of Sciences, Beijing 100190
Yafeng Bi
Institute of Acoustics, Chinese Academy of Sciences
Zhaoyong Sun
Key Laboratory of Noise and Vibration Research, Institute of Acoustics, Chinese Academy of Sciences
Jun Yang
Key Laboratory of Noise and Vibration Research, Institute of Acoustics, Chinese Academy of Sciences, Beijing 100190

Article

Keywords: acoustics structure design, deep learning, multiorder Helmholtz resonator, sound insulation

Posted Date: February 26th, 2021

DOI: https://doi.org/10.21203/rs.3.rs-255615/v1

Acoustic Structure Inverse Design and Optimization Using Deep Learning

Xuecong Sun[1,2], Han Jia[2,3*], Yuzhen Yang[1], Han Zhao [1,2], Yafeng Bi[1], Zhaoyong Sun[1] and Jun Yang[1,2*]

[1] Key Laboratory of Noise and Vibration Research, Institute of Acoustics, Chinese Academy of Sciences, Beijing 100190, People's Republic of China

[2] University of Chinese Academy of Sciences, Beijing 100049, People's Republic of China

[3] State Key Laboratory of Acoustics, Institute of Acoustics, Chinese Academy of Sciences, Beijing 100190, People's Republic of China

[*] Authors to whom correspondence should be addressed: hjia@mail.ioa.ac.cn and jyang@mail.ioa.ac.cn

Keywords: acoustics structure design, deep learning, multiorder Helmholtz resonator, sound insulation

Abstract

From ancient to modern times, acoustic structures have been used to control the propagation of acoustic waves. However, the design of acoustic structures has remained a time-consuming and computational resource-consuming iterative process. In recent years, deep learning has attracted unprecedented attention for its ability to tackle hard problems with large datasets, achieving state-of-the-art results in various tasks. In this work, an acoustic structure design method is proposed based on deep learning. Taking the design of multiorder Helmholtz resonator as an example, we experimentally demonstrate the effectiveness of the proposed method. Our method is not only able to give a very accurate prediction of the geometry of acoustic structures with multiple

strong-coupling parameters, but also capable of improving the performance of evolutionary approaches in optimization for a desired property. Compared with the conventional numerical methods, our method is more efficient, universal and automatic, and it has a wide range of potential applications, such as speech enhancement, sound absorption and insulation.

1. Introduction

Acoustic structures have been used for centuries to control acoustic waves in terms of amplitude and phase. With extensive achievements in fabrication technology, unprecedented functionalities can be obtained by designing and engineering artificial structures with more complex properties. Recently, many exotic functionalities, such as anomalous refraction/reflection[1,2], invisibility[3,4], and novel acoustic sensing[5], have been realized with fantastic acoustic structures. However, the development of accurate and computationally efficient design and optimization approaches for the acoustic structures is still in the early stages. During the design process, the forward calculation, i.e., predicting the acoustic properties based on the acoustic structures, is well understood with analytical and numerical approaches, such as the lumped-parameter techniques (LPTs), transfer matrix method (TMM) and finite element method (FEM). Nevertheless, the inverse problem, i.e., inferring acoustic structures from on-demand acoustic properties, is currently a prohibitive task even with the most advanced numerical tools. To search the formidably large design space efficiently, the inverse design procedure is usually guided by optimization algorithms, such as gradient-based

approaches and evolutionary approaches. As structural complexity grows, the above methods will take a prohibitive amount of time, which seriously limits the usefulness of such approaches. Therefore, it is of great significance to identify an efficient, universal and automatic acoustic structure design method.

In recent years, deep learning (DL) has emerged as a very powerful computational method. In light of its exceptional success in domains related to computer science and engineering[6–10], DL has attracted increasing attention from researchers in other disciplines, including materials science[11], chemistry[12], physics[13–15], computational imaging[16,17] and microscopy[18]. Moreover, DL has become a radically new approach in the context of photonic and electromagnetic design, such as approximation of light scattering from plasmonic nanostructures[19–22] and inverse design of the electromagnetic metasurface structure[23], over the past few years. Recently, DL has also been used to solve the inverse problem of the variable cross-sectional acoustic structure[24] and two-dimensional acoustic cloaking[25]. However, both the researches trained the deep neural networks (DNNs) for specific structures, which are hard to be extended to other acoustic structures.

In view of the current problems and previously reported designs, here we propose an efficient, universal and automatic acoustic structure design method to solve the inverse problem. In our method, we analyze acoustic structures by LPT and develop connections between geometric parameters (GPs) and equivalent electrical parameters (EEPs). Then, a DNN is set up and trained to determine the inner rules between the EEPs of the acoustic structures and their acoustic properties. To evaluate the

effectiveness of the proposed design method, a multiorder Helmholtz resonator (HR) is designed to realize acoustic insulation at specific frequencies (see Fig. 1). Once design requirements are input into the trained model, the EEPs of the structures will be generated quickly and automatically. Then, the GPs can be calculated through the LPT. In this example, it has been proven that the trained DNN can not only solve the inverse design problems of acoustic structures more quickly than its numerical counterpart, but also improve the performance of evolutionary approaches in optimization for a desired property. Finally, we design an acoustic filter (AF) to decrease the line-spectrum noise using the proposed design method. This DL approach is an effective design tool for acoustic structure on-demand design and optimization. Considering that various acoustic structures can be analyzed by the LPT exactly in the low frequency range, the proposed approach has a strong versatility and scalability, which can be further extended to other acoustic structures.

2. Result

2.1. Physical Model

Owing to the excellent characteristics of manipulating low-frequency sound waves with subwavelength dimensions, acoustic structures based on HRs have emerged as an attractive option in various fields such as sound proofing[26,27], asymmetric sound transmission[28], sound metadiffusers[29], and acoustic superlens[30,31] et al. However, traditional HRs support only one monopolar resonant mode with a narrow bandwidth. Therefore, the application of constructed functional devices has been restricted. In the latest research, the multiorder HR, which can generate multiorder resonances, was

presented to compensate for the above deficiencies[32]. Figure 1b shows a schematic view of a two-order Helmholtz resonator (THR). The acoustic properties of the THR can be analyzed by the LPT exactly. The relationship between GPs $gp = [a_1, l_1, r_1, h_1, a_2, l_2, r_2, h_2]$ and EEPs $rmc = [R_1, M_1, C_1, R_2, M_2, C_2]$ is shown in Table 1. Therefore, the forward problem of the THR model can be solved satisfactorily through the LPT. The acoustic impedance of the THR can be written as follows:

$$Z_{THR} = R_1\sqrt{\omega} + j\omega M_1 + \frac{1}{j\omega C_1 + \dfrac{1}{R_2\sqrt{\omega} + j\omega M_2 + 1/j\omega C_2}}, \quad (1)$$

where $\omega = 2\pi f$ is the angular frequency. From Eq. (1), the THR with two neck-and-cavity substructures can induce two discrete resonant modes. Therefore, when the THR is placed as a side branch of a tube, there are two sound transmission loss (STL) peaks corresponding to the two resonant modes which are shown in Fig. 1b.

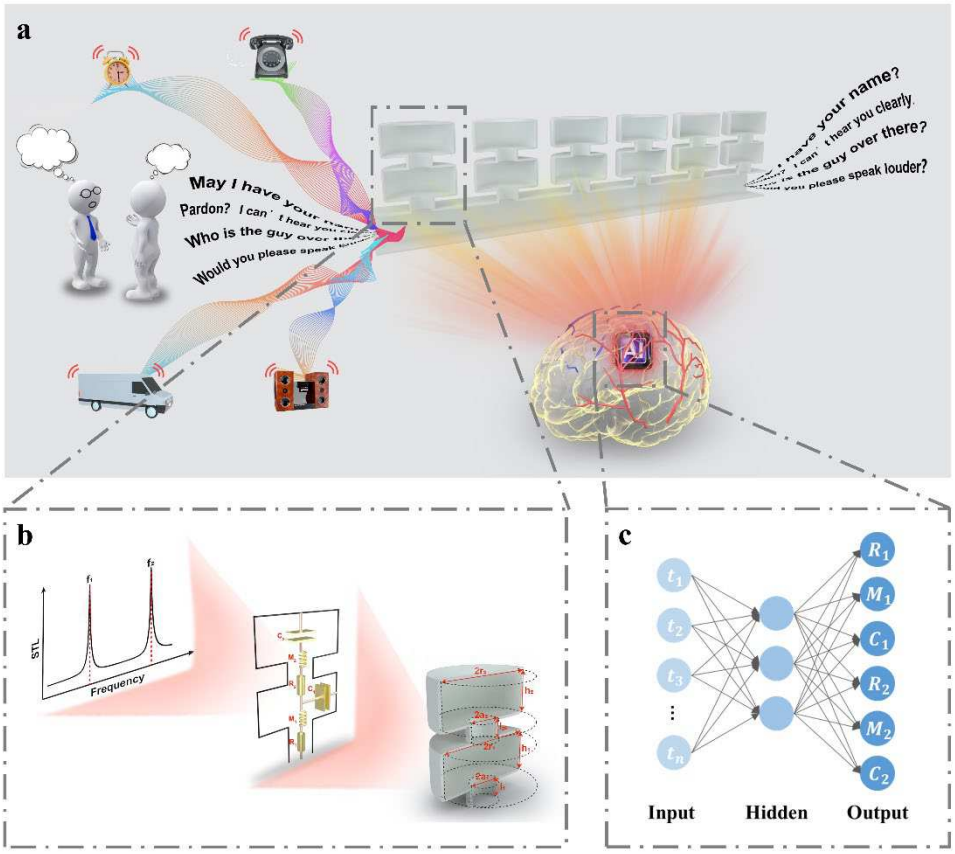

Fig. 1 Acoustic structure design method based on the DL. (a) The proposed DL approach can realize the on-demand design of the acoustic structures. For example, the DL approach can be used to design the THRs. The THRs are placed as a side branch of a tube, which can be used to filter out the background noise and make the speech clearer. Here, the cross section of the tube is $S = 100\ cm^2$. (b) Schematic view of the THR: The THR is constructed by neck-and-cavity substructures of two elements arranged in a cascade way. The i^{th}-order cavity is equivalent to the acoustic compliance C_i. The i^{th}-order neck is equivalent to the acoustic inertance M_i and the acoustic resistance R_i. Here, $a_i$and r_i are the radii of the cylindrical necks and cavities, respectively; l_i and h_i are the lengths of the cylindrical necks and cavities, respectively. In this work, the ranges of the GPs are set as $0.1cm < a_i < 2.5cm$, $0.1cm < l_i < 5cm$ and $0.1cm < h_i < 12.7cm$ $(i = 1,2)$, and the radii of the cavities are set as $r_1 = r_2 = 5cm$; the ranges of the EEPs are set as $1 < R_i < 170$, $1 < M_i < 300$ and $7 \times 10^{-10} < C_i < 7 \times 10^{-9}$ $(i = 1,2)$. When the THR is placed as a side branch of a tube, there are two STL peaks corresponding to the two resonant frequencies f_1 and f_2. (c) The THRs are designed by a trained DNN. The DNN has a cascaded structure of many layers of nonlinear processing units, where each layer uses the output from

the previous layer as input.

In practical applications such as sound insulation, we usually design acoustic structures according to noise spectra. That is, we need to infer the EEPs of the THR from a measured or desired STL spectrum. However, solving this inverse problem is still a major challenge, because we must solve a six-degree equation of resonant frequency during the inverse design process (see Method). The classical Abel–Ruffini theorem states that the general univariate polynomial equation of degree d is solvable by radicals if and only if d is less than five[33]. Therefore, no analytical solution of the inverse design problem of THR is known, and numerical methods need to be used. Considering that the inverse design problem of THR involves multiple strong-coupling parameters, DNN is suitable for avoiding time-consuming numerical methods in the design process.

$GP \rightarrow RMC$	$RMC \rightarrow GP$
$\boldsymbol{R_i = l_i\sqrt{2\eta\rho_0}/\pi a_i^3}$	$\frac{\rho_0 R_i}{\sqrt{2\eta\rho_0}}a_i^2 - \left(\frac{8\rho_0\beta_i}{3r_i\pi^2} + M_i\right)a_i + \frac{16\rho_0}{3\pi^2} = 0$
$\boldsymbol{M_i = \rho_0(l_i + \delta_i)/\pi a_i^2}$	$l_i = \frac{3\pi R_i a_i}{\sqrt{2\eta\rho_0}}$
$\boldsymbol{C_i = V_i/\rho_0 c_0^2}$	$V_i = C_i\rho_0 c_0^2$

Table 1 Relationship between GPs and EEPs. Here, $V_i = \pi r_i^2 h_i$ is the volume of the i^{th}-order cavity ; ρ_0 is the static air density; c_0 is the sound speed; and η is the viscosity of air. $\delta_i = \frac{8a_i}{3\pi}(2 - \beta_i\frac{a_i}{r_i})$ is the end correction associated with the inner and outer openings of the i^{th}-order neck, where $\beta_1 = 0.75$ and $\beta_2 = 1.05$ are the correction factors ($i = 1,2$). The values of the physical constants can be seen in Table S2.

Our goal is to use a DNN to solve the inverse design problem of the STL spectrum. The EEPs, that would most closely produce the target STL spectrum, can be determined based on the trained DNN. The GPs can be calculated based on the EEPs through the LPT (see Table 1). Here, we propose a fully-connected neural network as shown in Fig. 1c. A desired STL spectrum $t = [t_1, t_2, t_3, \dots, t_n]$ is taken as the input. The STL spectrum is sampled from 101 Hz to 600 Hz with a step of 1 Hz. Thus, the number of inputs is n = 500. The outputs $rmc = [R_1, M_1, C_1, R_2, M_2, C_2]$ are the EEPs corresponding to the designed structure.

The datasets were generated using LPT. To generate a sample, first, we sampled randomly within the given ranges of the GPs and obtained a group of GPs. Next, the EEPs and the STL spectrum could be calculated through the LPT (see Method). To make the model training easier, the samples should have good performance in sound isolation and be distribute uniformly in the frequency range of interest. Therefore, the samples were selected during the process of data generation (see Method). Figure 2a shows the distribution of the filtered samples. The two resonant frequencies f_1 and f_2 of the samples in the datasets cover the frequency range of interest. The average value of the STL at the resonant frequency $\frac{t(f_1)+t(f_2)}{2}$ is over 10 dB.

The dataset, which contained 195000 samples, was split into training, validation and test sets (80%, 10% and 10%, respectively) to train the DNN. The inputs were normalized, shuffled and then fed into the network, which can accelerate convergence of the algorithm. The mean square error (MSE) was used to represent a loss function between the normalized and desired output. The train loss was used to generate the

gradients, and the network weights were updated by the Adam algorithm to minimize the discrepancy[34]. The hyperparameters (for example, number of hidden layers, neurons and learning rate) were set according to the performance on the validation set. We utilized the batch normalization technique to improve the convergence speed of the training[35]. In addition, the dropout regularization technique was employed to avoid overfitting[36]. Ultimately, a fully connected network with three hidden layers was selected. The numbers of neurons of each hidden layer are 450, 250 and 220 respectively. The learning rate is set as 0.001, and the batch size is set as 256. We stopped training when the validation loss stopped decreasing, and the learning curve of the DNN on the validation set is shown in Fig. 2b. The rapidly decreasing MSE of validation instances shows that training is highly effective. The test set is used to evaluate the generalization capability of the trained DNN. And the prediction results on the test set can be found in S2 of the Supplementary Information. It should be noted that these parameters were not heavily optimized, and more efficient schemes can certainly be found.

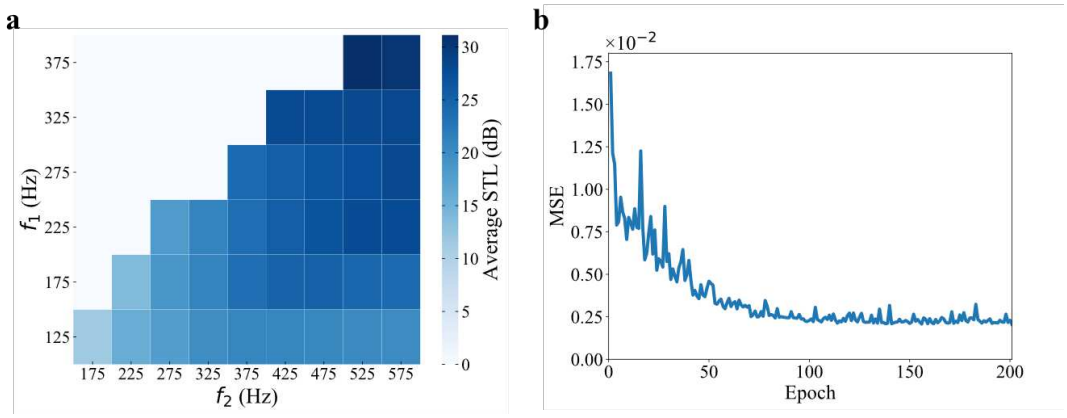

Fig. 2 Distribution of samples and learning curve of the DNN. (a) Average STL distribution at the resonant frequencies: f_1 and f_2 are the first order and second-order resonant frequencies of the THR,

respectively. The color of each square represents the average STL of the samples in the 50 Hz bandwidth centered in the corresponding resonant frequency. (b) The MSE of validation set over the epoch.

2.2. DNN solves the problem of THR inverse design.

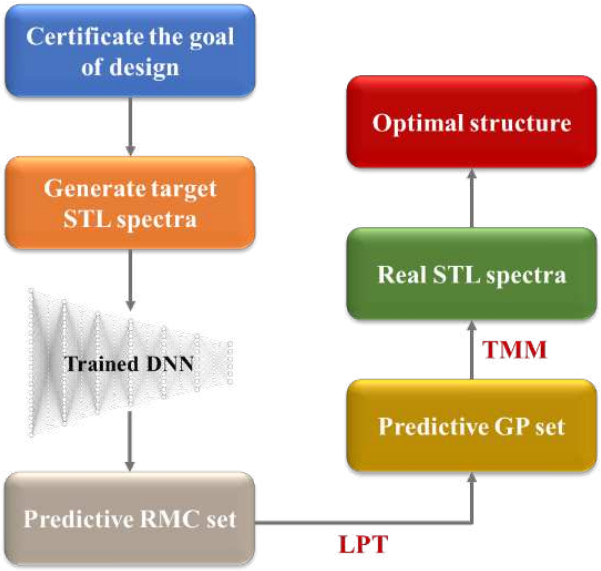

Fig. 3 Concept schematic of the design process.

Here, we show an example of designing the structure of THR using the trained DNN to realize acoustic insulation at specific frequencies. The concept schematic of the design process is shown in Fig. 3. First, we need to certificate the goal of the design. Here, the target resonant frequencies are set as $f_1^{\text{target}} = 150\text{Hz}$ and $f_2^{\text{target}} = 250\text{Hz}$, where the values of the STL are at least 10 dB. Therefore, we can generate a group of curves as the desired STL spectra according to the requirements, even though most of the spectra may not have a corresponding structure. We feed these spectra into the trained DNN and obtain the predictive RMC parameters. Then, the GPs can be calculated through the LPT. Finally, we can calculate the real STL spectra by the TMM (see S1 of the Supplementary Information) and select the most qualified structure.

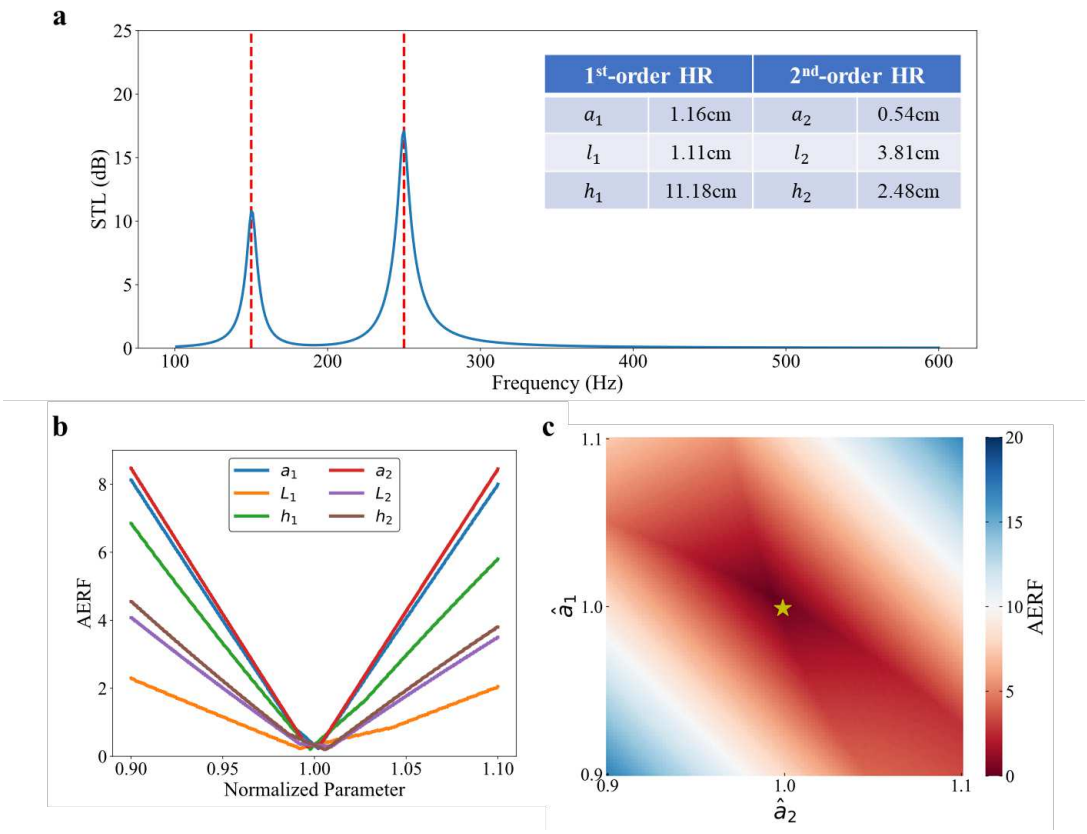

Fig. 4 Results of the inverse design. (a) STL spectrum of the selected THR structure calculated by the TMM (blue solid line). The target resonant frequencies 150 Hz and 250 Hz are marked by the red dotted lines. The GPs of the selected THR structure are shown in the inset. (b) AERF varies with the GPs. The radii of the cylindrical necks a_i (i = 1,2), the lengths of the cylindrical necks l_i (i = 1,2) and the lengths of the cavities h_i (i = 1,2) all have an impact on the resonant frequencies. (c) Average design error of the selected structure (yellow star) when the radii of the two cylindrical necks (a_1, a_2) are perturbed. $\hat{a}_1$ and $\hat{a}_2$ are the normalized radii, which can be presented as $\hat{a}_1 = a_1/a_1^*$ and $\hat{a}_2 = a_2/a_2^*$, respectively. a_1^* and a_2^* are the radii of the two cylindrical necks of the selected structure. The other GPs of the structures used to draw the color map are the same as the selected structure.

Figure 4a shows the GPs and STL spectrum of the selected structure. There are two SPL peaks higher than 10 dB at 150 Hz and 250 Hz, which is in good agreement with the design requirements. All the six GPs $[a_1, l_1, h_1, a_2, l_2, h_2]$ affect the acoustic characteristics of the THR. Here, we use the average error of the resonant frequency

(AERF) to evaluate the sensitivity of the resonant frequency on different GPs, which can be expressed as $\mathrm{AERF}(gp) = \frac{\left|f_1(gp)-f_1^{\mathrm{target}}\right|+\left|f_2(gp)-f_2^{\mathrm{target}}\right|}{2}$. Here, $f_1(gp)$ and $f_2(gp)$ are the real resonant frequencies of the structure whose GPs are denoted as gp. In Fig. 4b, we show the AERF varying with the GPs. The resonant frequencies are more sensitive to changes in a_1 and a_2. Then, we choose these two parameters to analyze the optimality of the solution provided by our DNN. In the analysis, the radii of the cylindrical necks a_1 and a_2 of the selected structure are changed within the range of $\pm 10\%$, while other GPs are unchanged. Then, we obtained a group of new structures around the selected structure and calculated their AERFs of them. Figure 4c shows the AERFs, which can be regarded as a function of a_1 and a_2. It is clear that the selected structure provided by the trained DNN is almost the optimal solution within the range of observations, which demonstrates the accuracy of the proposed design technology.

2.3. DNN aided optimization method

In section 2.2, we focus mainly on the design precision of the resonant frequencies of the structure, while the value of the STL at the resonant frequencies is just slightly higher than 10 dB. In practical applications, the sound insulation effects are usually expected to be as good as possible, and need to be realized through optimization methods[37]. One of the mainstream methods is through evolutionary algorithms such as genetic algorithm (GA)[38,39] and particle swarm optimization (PSO)[40]. However, evolutionary approaches always take a prohibitive amount of time, which greatly limits their usefulness. One of the reasons is that the initial condition of the algorithms is not good enough, so we often need to search the parameter space over dozens/hundreds of

generations to gradually approach the optimization target. Now that an arbitrary STL spectrum can be designed using the proposed DNN with little effort, we can further use it to provide a good initial condition for the evolutionary algorithms, i.e., the initial population would include a certain number of elitist individuals provided by DNN. This step can be regarded as providing a prior knowledge for optimization problems.

Here, we want to maximize the average value of the STL at the target resonant frequencies, which can be recast as

$$\begin{aligned} \min_{gp} J = \min_{gp} -[t(f_1^{\text{target}}, gp) + t(f_2^{\text{target}}, gp)] \\ s.t.\ t(f_1^{\text{target}}, gp) > 10dB \ \ and \ \ t(f_2^{\text{target}}, gp) > 10dB, \end{aligned} \tag{2}$$

where f_1^{target} and f_2^{target} are still set as 150 Hz and 250 Hz, respectively; $t(f_1^{\text{target}}, gp)$ and $t(f_2^{\text{target}}, gp)$ are the values of the STL at the target resonant frequencies of the THR, whose GPs are denoted as gp. The optimizations are realized by GA under two initialization conditions. In the first case, the initial population includes 50 individuals that are generated randomly, i.e., we have no prior knowledge about the optimization. In the second case, the initial population includes 45 randomly generated individuals and 5 elitist individuals. The elitist individuals, whose resonant frequencies are 150 Hz and 250 Hz, are generated by the proposed DNN. This task is nonrecurring, and each elitist individual requires only a query of the DNN, which takes no more than a few milliseconds. For comparison, the other algorithmic parameters remain the same. We receive the most optimized individual after 50 generations in the evolution. The comparison of the optimization effect under the two conditions is shown in Fig. 5. A good initial condition can not only effectively accelerate convergence

velocity, but also improve the results of the optimization. Therefore, the DNN-aided optimization method is feasible and more efficient for optimizing the acoustic structure. Details about the optimization can be found in S3 of the Supplementary Information.

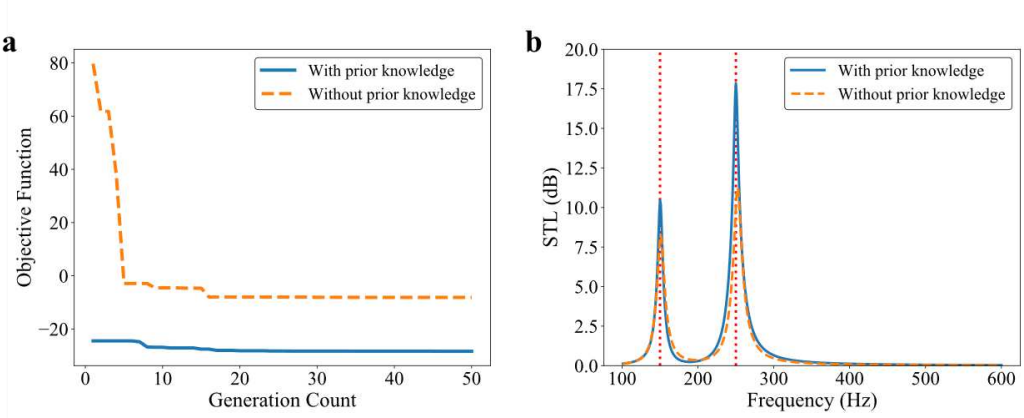

Fig. 5 The optimization effect through the GA with and without prior knowledge. (a) Comparison of the decreasing process of the objective function J under the two conditions (with prior knowledge, blue solid line; without prior knowledge, yellow dotted line). Considering that the initial population with prior knowledge includes a certain number of elitist individuals, the blue solid line converges faster than the yellow dotted line. (b) Comparison of the STL spectra of the optimal structures under the two conditions (with prior knowledge, blue solid line; without prior knowledge, yellow dotted line). The average STL at the target resonant frequencies with prior knowledge (14.2 dB) is higher than the average STL at the target resonant frequencies without prior knowledge (9.6 dB).

2.4. On-demand design of the acoustic filter

In practical applications, we need to filter out the multi-frequency line-spectrum noise in the background environment, and even achieve broadband sound insulation in a certain frequency range, requiring us to design a combined filter for specific noise frequencies. The traditional design method needs to perform the optimization for each noise frequency, so the efficiency is very low. In comparison, it takes only a few seconds to complete the design process using our design strategy. Here, we demonstrate an

example of designing an AF to decrease the line-spectrum noise at four frequencies: 150 Hz, 200 Hz, 250 Hz and 300 Hz. To realize four resonant frequencies, the AF is a combination of two THRs. The two THRs were designed using the DNN approach mentioned in section 2.2, with the photo and GPs shown in Fig. 6a. The STL spectrum of the AF, which is shown in Fig. 6b, is measured in a square standing wave tube (see Method). There are four transmission loss peaks at 150 Hz, 200 Hz, 250 Hz and 300 Hz, corresponding to the four resonant modes of the two THRs. These results confirm the design is very precise.

To evaluate the effectiveness of the AF, a pure voice mixed with noise at the above frequencies impinges from the left port of a square tube. A microphone is used to receive the signal at the right port of the waveguide. We performed the measurements with and without AF as a side branch of the tube. The time-domain waveform and the spectrogram of the signal filtered by the AF are shown in Fig. 6d and f, respectively. For comparison, the time-domain waveform and the spectrogram of the unfiltered signal are shown in Fig. 6c and e, respectively. The proposed AF significantly decreases the line-spectrum noise and improves the speech clarity of the original signal (the sound before and after filtering can be heard in the Supplementary Video). The experimental results prove that our approach can achieve the on-demand design of AF for many applications, such as noise reduction of the engine, helicopter and UHV transformers.

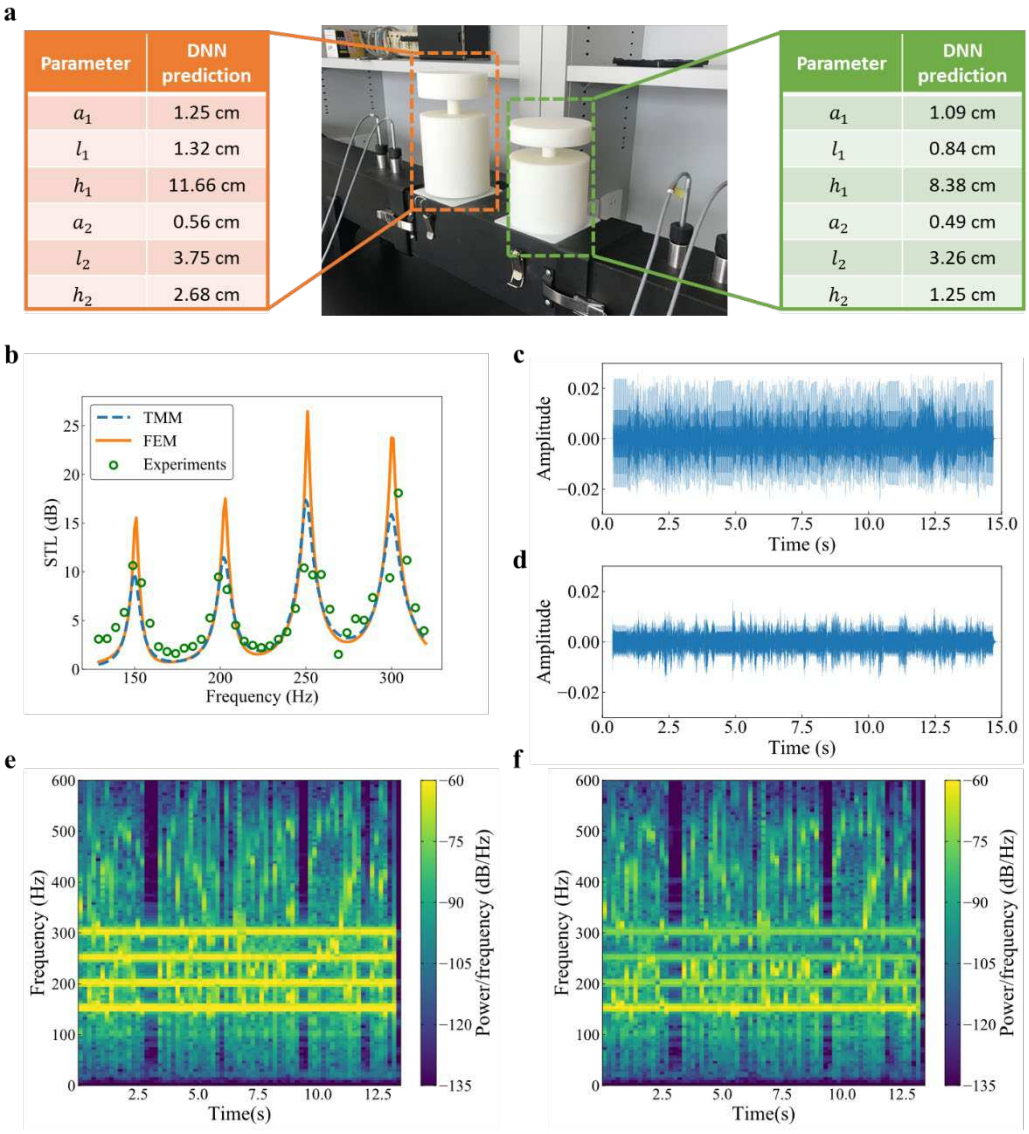

Fig. 6 Structure and experimental results of the AF. (a) Photo and GPs of the AF. Left inset: The GPs of the THR whose resonant frequencies are 150 Hz and 250 Hz. Right inset: The GPs of the THR whose resonant frequencies are 200 Hz and 300 Hz. (b) STL spectrum of the AF. The theoretical (blue dotted line, calculated by the TMM), simulated (orange solid line, calculated by the FEM) and experimental (green circles) results are consistent. (c) and (d) are the time-domain waveforms of the test signal before and after filtering, respectively. (e) and (f) are spectrograms of the test signal before and after) filtering, respectively.

3. Discussion

In this paper, we introduce a novel DL approach for acoustic structure design based

solely on desired acoustic properties. We designed, trained and tested the proposed design method, which shows a very accurate prediction of the geometry of acoustic structures with multiple strong-coupling parameters. Moreover, the trained model can also be used to aid evolutionary algorithms in completing the optimization task more efficiently. Compared with the conventional method, the proposed DL approach shows a significant improvement in efficiency, an acceleration of the design process and an obvious reduction in both computational and man-powered resources. The trained model would be an effective design tool for designers, especially for layman users who have less professional knowledge about acoustics. Moreover, the trained model can determine the inner rules between the EEPs and acoustic properties. Therefore, it can be easily extended to other acoustic structures that can be analyzed by the LPT. The effectiveness of the structures designed by our approach was evaluated through acoustic experiments, which promise a wide range of potential applications, such as speech enhancement, sound absorption and insulation, for the proposed DL approach.

Method

Lumped-parameter techniques for the THR: As mentioned in section 2.1, the THR can be satisfactorily and simply analyzed by the LPT[41]. The acoustic impedance of the THR can be written as Eq. (1). When the THR is a side branch of a tube, the STL can be expressed as:

$$t = 10\log\frac{X_b^2 + \left(\frac{Z_0}{2S} + R_b\right)^2}{R_b^2 + X_b^2}, \tag{3}$$

where R_b and X_b are the real part and imaginary part of Z_{2-HR}, respectively; $Z_0 = \rho_0 c_0$ is the acoustic impedance of the air; and S is the cross section of the tube. Eq. (3) shows that STL reaches its maximum value when the imaginary part $X_b = 0$. Therefore, we let $X_b = 0$ and simplify the equation. Then, a six-degree equation can be obtained:

$$\begin{aligned} M_1 C_1^2 M_2^2 \omega_0^6 + M_1 C_1^2 R_2^2 \omega_0^5 - C_1 M_2 \left(2M_1 \frac{C_1 + C_2}{C_2} + M_2\right) \omega_0^4 - C_1 R_2^2 \omega_0^3 \\ + \left[M_1 \left(\frac{C_1}{C_2}\right)^2 + 2(M_1 + M_2) \frac{C_1}{C_2} + M_1 + M_2\right] \omega_0^2 - \frac{C_1 + C_2}{C_2^2} = 0, \end{aligned} \tag{4}$$

where ω_0 is the resonant angular frequency. No analytical solution of the Eq. (4) is known, and the parameters in Eq. (4) are strongly coupled.. Therefore, solving the inverse problem remains a major challenge, and DNNs are trained to assist in the design process.

Data preparation: To generate a sample, first, we sampled randomly within the given ranges of GPs and obtained a group of GPs. Next, the EEPs and STL spectrum can be calculated through the LPT. If the EEPs is in the given ranges and the values of the STL at the resonant frequencies are over 10 dB, the sample is selected for the dataset. Moreover, to ensure that the distribution of the samples is as uniform as possible, the samples were classified into several groups based on their resonant frequencies. Each group is guaranteed to contain 5000 samples. More details about the data distribution can be found in Table S1 of the Supporting Information.

Numerical simulations: In this paper, FEM simulations were performed to verify the feasibility of our design by using the pressure acoustic module and thermoviscous

acoustic module of COMSOL Multiphysics. Plane wave radiation is set on the left side of the calculated fluid domain of the tube. The mesh type is the tetrahedral mesh, and the largest mesh element size was smaller than 1/6 of the shortest incident wavelength, and the further refined meshes were applied in the cylindrical necks.

Experimental measurements: The experimental THR samples were fabricated using 3D printing technology with a wall thickness of 5 mm. The material used for the samples is Lasty-KS, a type of UV-curable resin, with density of 1.13 g/cm^3. The acoustic impedance of the Lasty-KS is much larger than the acoustic impedance of air, so the wall of the THR can be regarded as rigid for the sound wave.

The layout of the measurement system is shown in Fig. 6. The two THRs were placed as a side branch of a square tube, where the connection was sealed by plasticene. As shown in Fig. 6b, the STL spectrum was measured using four 1/4-inch microphones (Brüel & Kjær, type-4187). The experimental measurements were conducted by the two-load method in a square standing wave tube, where the hard wall and acoustic sponge (as an anechoic boundary) were separately used at the terminal. When the mixed signals shown in Fig. 6d and e were measured, a pure voice mixed with noise impinged from the left port of the square tube. A 1/2-inch microphone (Brüel & Kjær, type-4189) was placed at the right port of the tube to receive the signal, while an acoustic sponge was used as the anechoic boundary at the right port.

References

1. Yang, Y., Jia, H., Bi, Y., Zhao, H. & Yang, J. Experimental demonstration of an

acoustic asymmetric diffraction grating based on passive parity-time-symmetric medium. *Phys. Rev. Appl.* **12**, 034040 (2019).

2. Yang, Y., Jia, H., Wang, S., Zhang, P. & Yang, J. Diffraction control in a non-Hermitian acoustic grating. *Appl. Phys. Lett.* **116**, 213501 (2020).

3. Bi, Y. *et al.* Experimental demonstration of three-dimensional broadband underwater acoustic carpet cloak. *Appl. Phys. Lett.* **112**, 223502 (2018).

4. Sun, Z., Sun, X., Jia, H., Bi, Y. & Yang, J. Quasi-isotropic underwater acoustic carpet cloak based on latticed pentamode metafluid. *Appl. Phys. Lett.* **114**, 094101 (2019).

5. Sun, X. *et al.* Sound Localization and Separation in 3D Space Using a Single Microphone with a Metamaterial Enclosure. *Adv. Sci.* **7**, (2019).

6. Hinton, G. *et al.* Deep neural networks for acoustic modeling in speech recognition: The shared views of four research groups. *IEEE Signal Process. Mag.* **29**, 82–97 (2012).

7. Krizhevsky, A., Sutskever, I. & Hinton, G. E. Imagenet classification with deep convolutional neural networks. *Commun. ACM* **60**, 84–90 (2017).

8. Cho, K. *et al.* Learning phrase representations using RNN encoder-decoder for statistical machine translation. *ArXiv Prepr. ArXiv14061078* (2014).

9. Silver, D. *et al.* Mastering the game of Go with deep neural networks and tree search. *nature* **529**, 484–489 (2016).

10.Socher, R., Chen, D., Manning, C. D. & Ng, A. Reasoning with neural tensor networks for knowledge base completion. *Adv. Neural Inf. Process. Syst.* **26**, 926–934 (2013).

11.Sanchez-Lengeling, B. & Aspuru-Guzik, A. Inverse molecular design using machine learning: Generative models for matter engineering. *Science* **361**, 360–365 (2018).

12.Goh, G. B., Hodas, N. O. & Vishnu, A. Deep learning for computational chemistry. *J. Comput. Chem.* **38**, 1291–1307 (2017).

13.Zahavy, T. *et al.* Deep learning reconstruction of ultrashort pulses. *Optica* **5**, 666–673 (2018).

14.Baldi, P., Sadowski, P. & Whiteson, D. Searching for exotic particles in high-energy physics with deep learning. *Nat. Commun.* **5**, 1–9 (2014).

15.Carrasquilla, J. & Melko, R. G. Machine learning phases of matter. *Nat. Phys.* **13**, 431–434 (2017).

16.White, A., Khial, P., Salehi, F., Hassibi, B. & Hajimiri, A. A Silicon photonics computational Lensless Active-flat-optics imaging System. *Sci. Rep.* **10**, 1–9 (2020).

17.Weng, J. *et al.* Meta-neural-network for real-time and passive deep-learning-based object recognition. *Nat. Commun.* **11**, 6309 (2020).

18.Rivenson, Y. *et al.* Deep learning microscopy. *Optica* **4**, 1437–1443 (2017).

19.Ma, W. *et al.* Deep learning for the design of photonic structures. *Nat. Photonics* 1–

14 (2020) doi:10.1038/s41566-020-0685-y.

20.Malkiel, I. *et al.* Plasmonic nanostructure design and characterization via Deep Learning. *Light Sci. Appl.* **7**, 1–8 (2018).

21.Sheverdin, A., Monticone, F. & Valagiannopoulos, C. Photonic Inverse Design with Neural Networks: The Case of Invisibility in the Visible. *Phys. Rev. Appl.* **14**, 024054 (2020).

22.Peurifoy, J. *et al.* Nanophotonic particle simulation and inverse design using artificial neural networks. *Sci. Adv.* **4**, eaar4206 (2018).

23.Qiu, T. *et al.* Deep learning: A rapid and efficient route to automatic metasurface design. *Adv. Sci.* **6**, 1900128 (2019).

24.Luo, Y.-T. *et al.* Probability-Density-Based Deep Learning Paradigm for the Fuzzy Design of Functional Metastructures. 11.

25.Ahmed, W. W., Farhat, M., Zhang, X. & Wu, Y. Deterministic and probabilistic deep learning models for inverse design of broadband acoustic cloak. *Phys. Rev. Res.* **3**,

26.Cheng, Y., Xu, J. Y. & Liu, X. J. One-dimensional structured ultrasonic metamaterials with simultaneously negative dynamic density and modulus. *Phys. Rev. B* **77**, 045134 (2008).

27.Fang, N. *et al.* Ultrasonic metamaterials with negative modulus. *Nat. Mater.* **5**, 452–456 (2006).

28.Li, Y. *et al.* Tunable asymmetric transmission via lossy acoustic metasurfaces. *Phys. Rev. Lett.* **119**, 035501 (2017).

29.Jiménez, N., Cox, T. J., Romero-García, V. & Groby, J.-P. Metadiffusers: Deep-subwavelength sound diffusers. *Sci. Rep.* **7**, 1–12 (2017).

30.Yang, X., Yin, J., Yu, G., Peng, L. & Wang, N. Acoustic superlens using Helmholtz-resonator-based metamaterials. *Appl. Phys. Lett.* **107**, 193505 (2015).

31.Xia, J. *et al.* Broadband tunable acoustic asymmetric focusing lens from dual-layer metasurfaces. *Phys. Rev. Appl.* **10**, 014016 (2018).

32.Long, H., Cheng, Y. & Liu, X. Reconfigurable sound anomalous absorptions in transparent waveguide with modularized multi-order Helmholtz resonator. *Sci. Rep.* **8**, 1–9 (2018).

33.Bernshtein, D. N. The number of roots of a system of equations. *Funct. Anal. Its Appl.* **9**, 183–185 (1979).

34.Kingma, D. P. & Ba, J. Adam: A method for stochastic optimization. *ArXiv Prepr. ArXiv14126980* (2014).

35.Ioffe, S. & Szegedy, C. Batch normalization: Accelerating deep network training by reducing internal covariate shift. *ArXiv Prepr. ArXiv150203167* (2015).

36.Srivastava, N., Hinton, G., Krizhevsky, A., Sutskever, I. & Salakhutdinov, R. Dropout: a simple way to prevent neural networks from overfitting. *J. Mach. Learn. Res.* **15**, 1929–1958 (2014).

37. Yang, M., Chen, S., Fu, C. & Sheng, P. Optimal sound-absorbing structures. *Mater. Horiz.* **4**, 673–680 (2017).

38. Tang, K. S., Man, K. F., Kwong, S. & He, Q. Genetic algorithms and their applications. *IEEE Signal Process. Mag.* **13**, 22–37 (1996).

39. Wang, T., Li, S. & Nutt, S. R. Optimal design of acoustical sandwich panels with a genetic algorithm. *Appl. Acoust.* **70**, 416–425 (2009).

40. Kennedy, J. & Eberhart, R. Particle swarm optimization. in *Proceedings of ICNN'95-International Conference on Neural Networks* vol. 4 1942–1948 (IEEE, 1995).

41. Pierce, A. D. *Acoustics: an introduction to its physical principles and applications*. (Springer, 2019).

Acknowledgements

This work is supported by the Key-Area Research and Development Program of Guangdong Province (Grant No. 2020B010190002), the National Natural Science Foundation of China (Grant No. 11874383), the Youth Innovation Promotion Association CAS (Grant No. 2017029) and the IACAS Young Elite Researcher Project (Grant No. QNYC201719).

Author contributions

J.Y. planned, coordinated, and supervised the project. X.S. and H.J. conceived the model. X.S. designed the algorithm and performed the theoretical and numerical calculations. X.S. and H.Z. participated in the experiments and data analysis. X.S. and H.J. jointly wrote the manuscript. All authors contributed to discussing the results and reading the manuscript.

Competing interests

The authors declare no competing interests.

Supporting Information

Supporting Information is available.

Figures

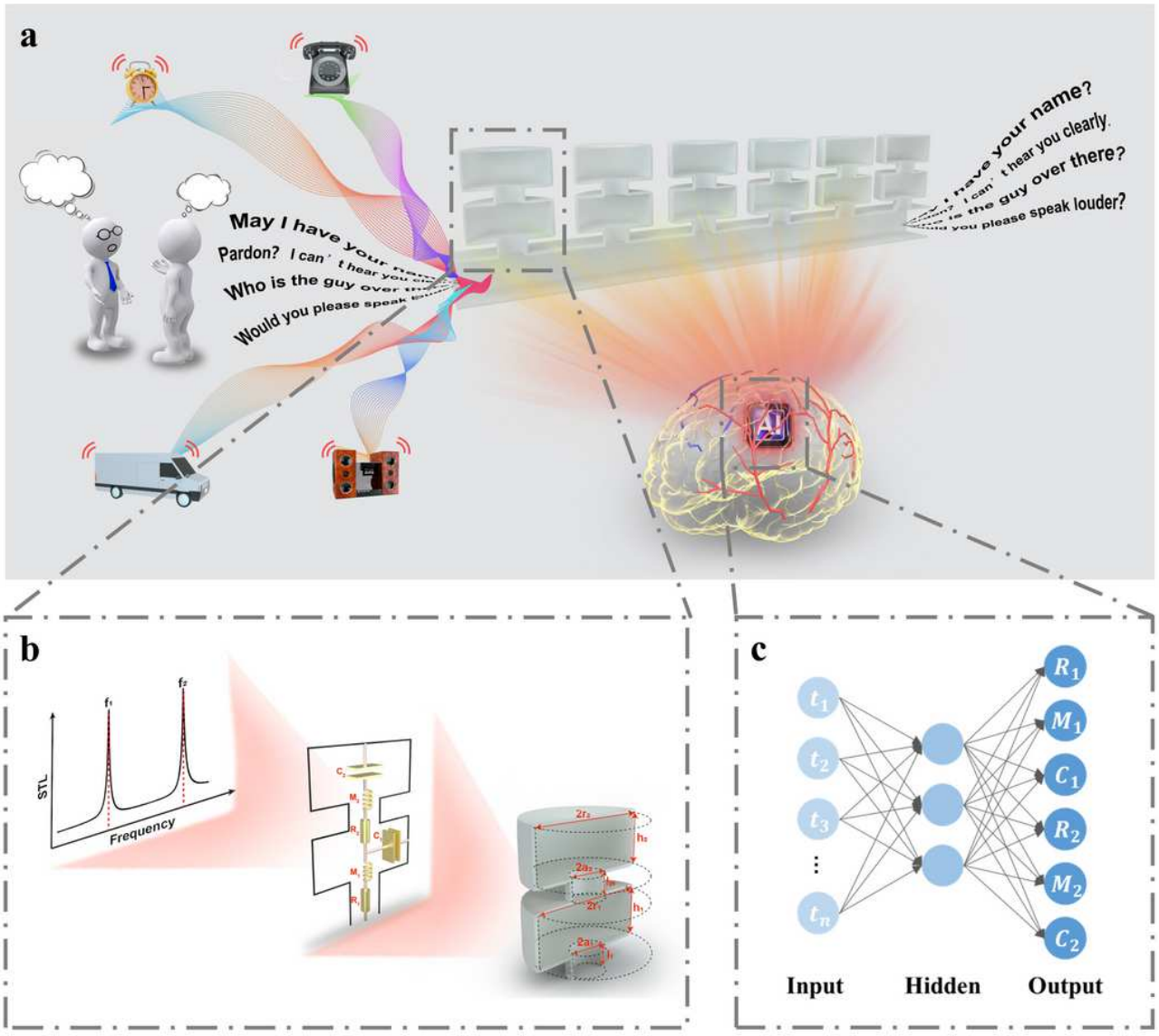

Figure 1

Acoustic structure design method based on the DL. (a) The proposed DL approach can realize the on-demand design of the acoustic structures. For example, the DL approach can be used to design the THRs. The THRs are placed as a side branch of a tube, which can be used to filter out the background noise and make the speech clearer. Here, the cross section of the tube is S=100 cm^2. (b) Schematic view of the THR: The THR is constructed by neck-and-cavity substructures of two elements arranged in a cascade way. The ith-order cavity is equivalent to the acoustic compliance C_i. The ith-order neck is equivalent to the acoustic inertance M_i and the acoustic resistance R_i. Here, a_iand r_i are the radii of the cylindrical

necks and cavities, respectively; l_i and h_i are the lengths of the cylindrical necks and cavities, respectively. In this work, the ranges of the GPs are set as 0.1cm□<a□_i<2.5cm, 0.1cm□<l□_i<5cm and 0.1cm<h_i<12.7cm (i=1,2), and the radii of the cavities are set as r_1=r_2=5cm; the ranges of the EEPs are set as 1<R_i<170, 1<M_i<300 and 7×10^(-10)<C_i<7×10^(-9) (i=1,2). When the THR is placed as a side branch of a tube, there are two STL peaks corresponding to the two resonant frequencies f_1 and f_2. (c) The THRs are designed by a trained DNN. The DNN has a cascaded structure of many layers of nonlinear processing units, where each layer uses the output from the previous layer as input.

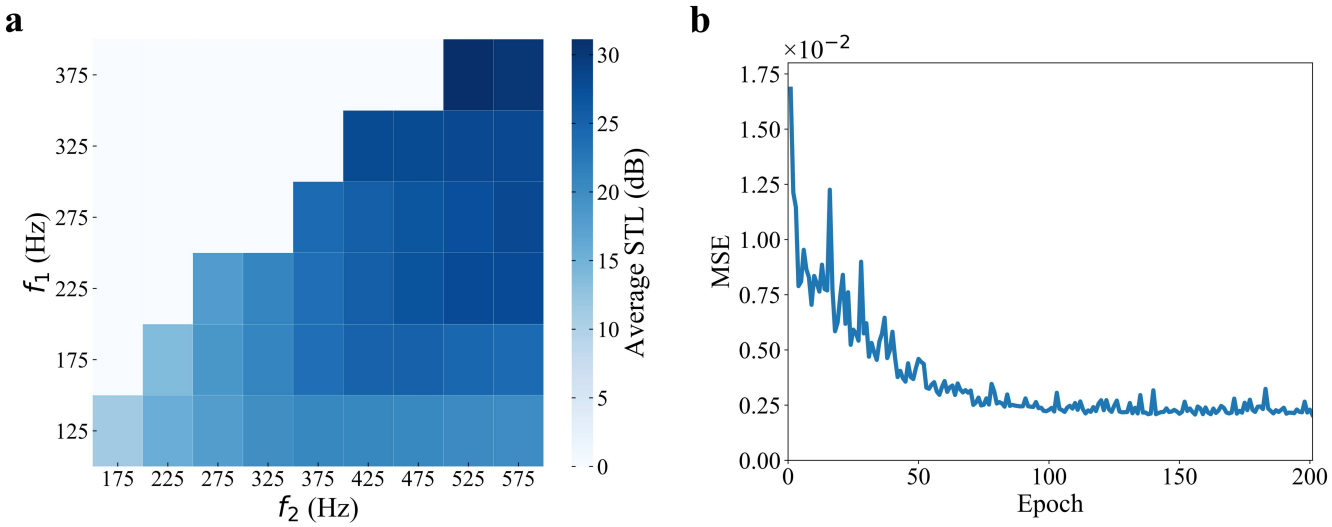

Figure 2

Distribution of samples and learning curve of the DNN. (a) Average STL distribution at the resonant frequencies: f_1 and f_2 are the first order and second-order resonant frequencies of the THR, respectively. The color of each square represents the average STL of the samples in the 50 Hz bandwidth centered in the corresponding resonant frequency. (b) The MSE of validation set over the epoch.

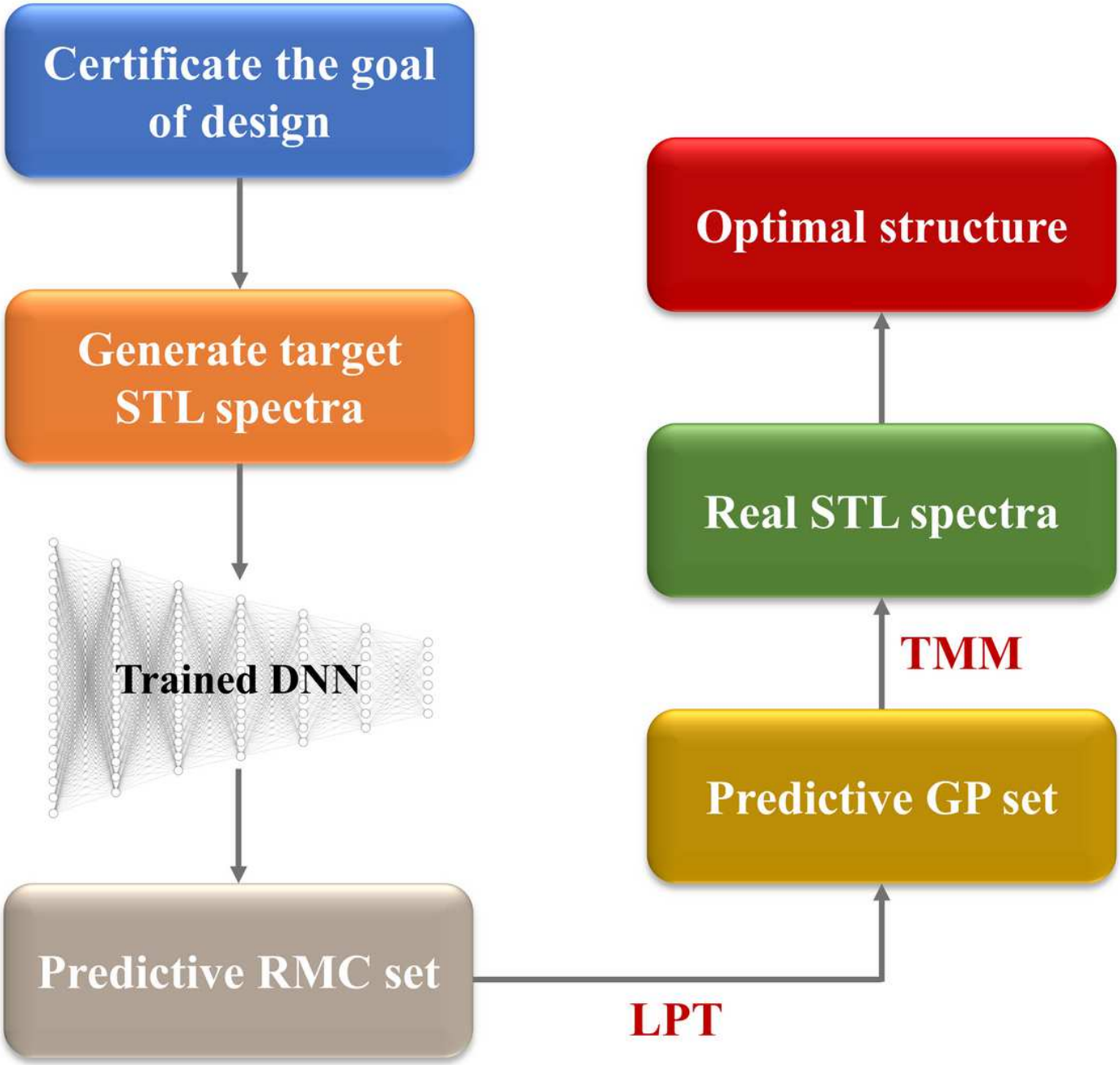

Figure 3

Concept schematic of the design process.

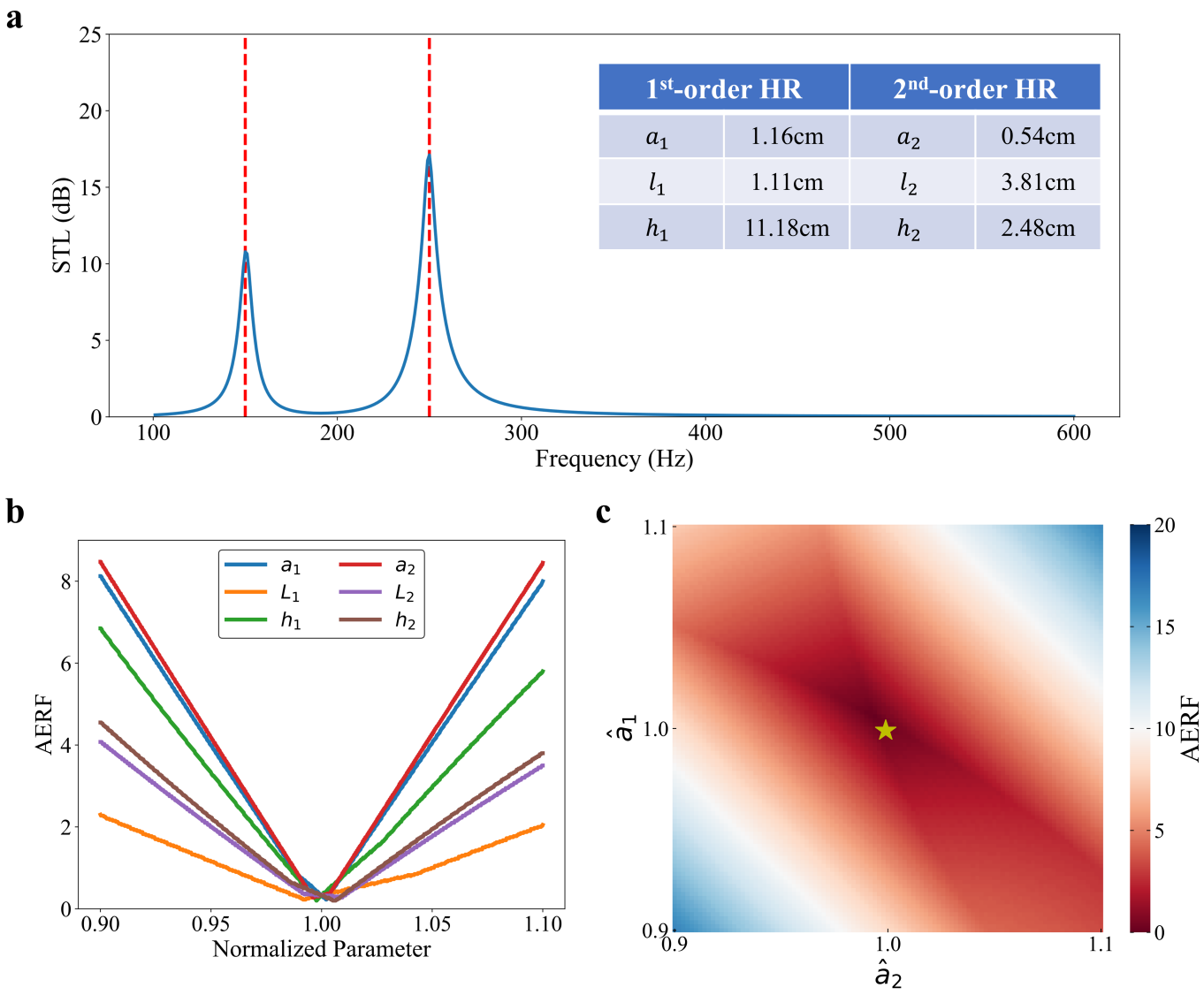

Figure 4

Results of the inverse design. (a) STL spectrum of the selected THR structure calculated by the TMM (blue solid line). The target resonant frequencies 150 Hz and 250 Hz are marked by the red dotted lines. The GPs of the selected THR structure are shown in the inset. (b) AERF varies with the GPs. The radii of the cylindrical necks a_i (i = 1,2), the lengths of the cylindrical necks l_i (i = 1,2) and the lengths of the cavities h_i (i = 1,2) all have an impact on the resonant frequencies. (c) Average design error of the selected structure (yellow star) when the radii of the two cylindrical necks (a_1,a_2) are perturbed. a □_1 and a □_2 are the normalized radii, which can be presented as a □_1=a_¹⁄(a_1^*) and a □_2=a_²⁄(a_2^*), respectively. a_1^* and a_2^* are the radii of the two cylindrical necks of the selected structure. The other GPs of the structures used to draw the color map are the same as the selected structure.

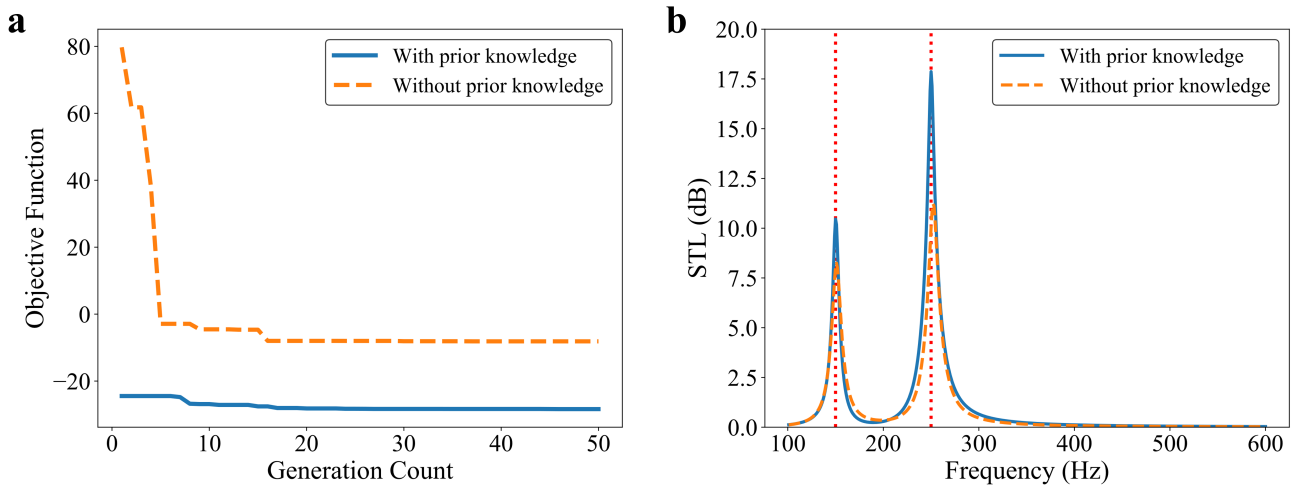

Figure 5

The optimization effect through the GA with and without prior knowledge. (a) Comparison of the decreasing process of the objective function J under the two conditions (with prior knowledge, blue solid line; without prior knowledge, yellow dotted line). Considering that the initial population with prior knowledge includes a certain number of elitist individuals, the blue solid line converges faster than the yellow dotted line. (b) Comparison of the STL spectra of the optimal structures under the two conditions (with prior knowledge, blue solid line; without prior knowledge, yellow dotted line). The average STL at the target resonant frequencies with prior knowledge (14.2 dB) is higher than the average STL at the target resonant frequencies without prior knowledge (9.6 dB).

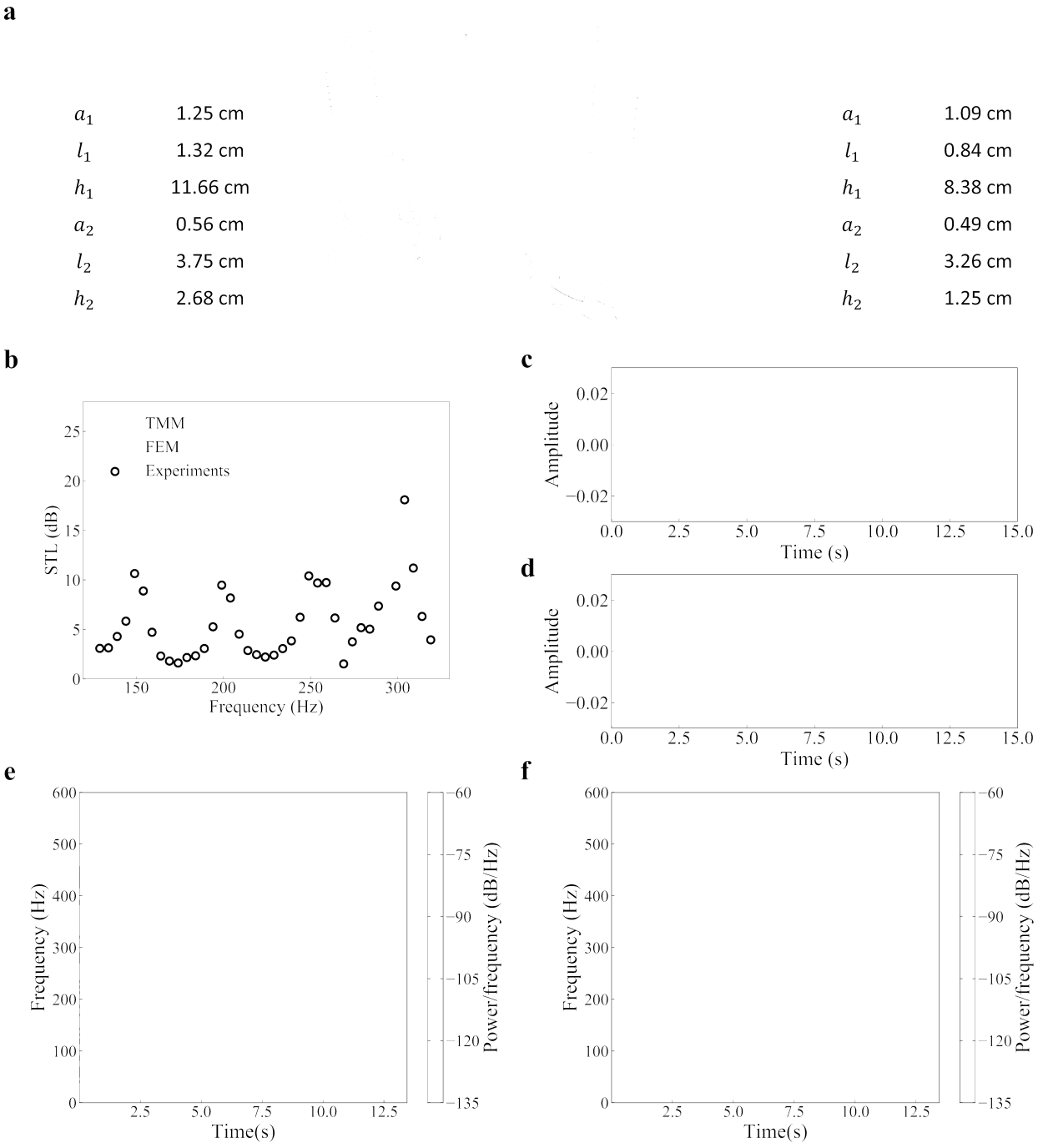

Figure 6

Structure and experimental results of the AF. (a) Photo and GPs of the AF. Left inset: The GPs of the THR whose resonant frequencies are 150 Hz and 250 Hz. Right inset: The GPs of the THR whose resonant frequencies are 200 Hz and 300 Hz. (b) STL spectrum of the AF. The theoretical (blue dotted line, calculated by the TMM), simulated (orange solid line, calculated by the FEM) and experimental (green circles) results are consistent. (c) and (d) are the time-domain waveforms of the test signal before and

after filtering, respectively. (e) and (f) are spectrograms of the test signal before and after) filtering, respectively.

Supplementary Files

This is a list of supplementary files associated with this preprint. Click to download.

- SupplementaryVideo.mp4
- SI.docx
- figureS1.tif
- figureS2.tif